High-throughput quantitative microscopy-based half-life measurements of intravenously injected agents

Laura G. Bracaglia[a,1], Alexandra S. Piotrowski-Daspit[a,1], Chun-Yu Lin[a], Zoe M. Moscato[a], Yongheng Wang[a], Gregory T. Tietjen[a,b], and W. Mark Saltzman[a,c,d,2]

[a]Department of Biomedical Engineering, Yale University, New Haven, CT 06511; [b]Department of Surgery, Yale School of Medicine, New Haven, CT 06511; [c]Department of Chemical and Environmental Engineering, Yale University, New Haven, CT 06511; and [d]Department of Cellular & Molecular Physiology, Yale School of Medicine, New Haven, CT 06511

Accurate analysis of blood concentration and circulation half-life is an important consideration for any intravenously administered agent in preclinical development or for therapeutic application. However, the currently available tools to measure these parameters are laborious, expensive, and inefficient for handling multiple samples from complex multivariable experiments. Here we describe a robust high-throughput quantitative microscopy-based method to measure the blood concentration and circulation half-life of any fluorescently labeled agent using only a small (2 μL) amount of blood volume, enabling additional end-point measurements to be assessed in the same subject. To validate this method, we demonstrate its use to measure the circulation half-life in mice of two types of fluorescently labeled polymeric nanoparticles of different sizes and surface chemistries and of a much smaller fluorescently labeled monoclonal antibody. Furthermore, we demonstrate the improved accuracy of this method compared to previously described methods.

quantitative microscopy | circulation half-life | drug delivery | nanoparticle

An accurate measurement of the time that an intravenously (IV) injected agent remains circulating in the blood, described by the circulation half-life, provides valuable insight into the activity of that agent in vivo. For example, prolonged blood circulation time is critical for many nanoparticle (NP)-based therapies intended for systemic IV injection; longer circulation time may increase the concentration of a NP therapeutic—particularly if targeted (for example, with antibodies conjugated to the surface)—at its intended site (1, 2). This is also true of other therapeutic agents, such as antibodies (3–5) and antibody-drug conjugates (6). In other applications where extended circulation time is not the desired outcome, knowing the circulation half-life could help in planning experimental time points that require a minimum level of biological activity in the blood. For example, fluorescently tagged antibodies injected IV can stain cells found in intraluminal vasculature (7), or a systemically injected agent can provide imaging contrast while circulating blood concentrations are still sufficient (8, 9).

The most commonly used, or "traditional," method to assess the circulating concentration of fluorescently labeled NPs in the blood is a three-part protocol consisting of blood collection, isolation of the fluorescent dye from the NP suspension in the blood, and then measurement of fluorescence intensity using a plate reader (2). This method is time-consuming and requires the researcher to trace the agent through several suspensions and concentrations which can introduce points of error. More importantly, this method typically utilizes 20 μL or more of blood in order to extract a detectable amount of fluorescent signal for measurement in a 96-well plate. The NIH Office of Animal Care and Use safe handling procedures restrict the circulating blood volume which can be removed in survival procedures to 1% every

24 h (10, 11). It is estimated that a 30-g mouse has 1.65 to 2.10 mL of blood, limiting the safe removal of blood to 17 to 21 μL daily. To comply with this constraint, multiple animals are often used to acquire time-point measurements of less than 1 d (12), which increases the variance, cost, and size of the experiment. Even in cases where greater blood volumes can be removed, this loss of volume results in significant loss of injected material from the circulation. For these reasons, most experiments use nonessential mice cohorts, like nontumor-bearing mice or mice that are otherwise not used for additional data acquisition (for example, therapeutic end-point measurements) (13–15). Notably, circulation half-life measured in nonexperimental mice or in mice that experience substantial blood loss could be significantly different from the half-life in experimental animals.

In response to these challenges, we have developed a method to accurately assess the concentration of any fluorescent agent in a blood sample volume of only 2 μL (16). This method can safely be used within NIH guidelines to collect up to 10 time points per day from a single animal, reducing both the experimental cohort size required for in vivo studies and the variability

Significance

The effectiveness of systemically delivered therapeutics is dependent on their residence time in circulation, as this parameter influences the frequency of interaction with intended target sites prior to elimination from the body. Consequently, measurements of circulation half-life in relevant animal models of disease can be essential to therapeutic design. We designed a high-throughput quantitative microscopy-based approach to accurately measure the blood concentration and circulation half-life of intravenously administered fluorescently labeled agents using only a small amount of blood volume. This platform can be used to analyze large sample volumes from multivariable studies without the need for specialized equipment or extensive sample processing and has the potential to significantly accelerate preclinical therapeutic screening.

www.manaraa.com

between measurements. Furthermore, this procedure results in a loss of less than 1% of blood volume and injected material over 10 time points. We therefore propose that this method can be used in conjunction with other experimental end points without significant alteration of results from material loss.

Recently, we demonstrated the measurement of circulating dye-loaded fluorescent NP concentration using quantitative microscopy of a 2-μL blood smear on a microscope slide (16). The varied thickness of the blood sample at different coordinates was accounted for by including a reference NP at a known concentration in the collected sample. This technique results in precise measures of NP concentration in the blood of several animals, but has the limitation of multiple sample preparation steps, limiting the throughput of the assay (16). In this current report, we significantly expand on this finding to show how this technique can be applied to a larger cohort of animals in a high-throughput multiwell plate analysis format without the need for a reference fluorescent agent. We show that this method can be combined with other end-point analyses such as biodistribution measurements and organ uptake studies, due to minimal material lost at each collection point. We find that this method is reproducible across different experiments and does not require special surgical or technical skill to execute. We also demonstrate that this method can be used for a variety of different therapeutic agents including different NP formulations and antibodies. We anticipate that this method could be applied to any fluorescently labeled agent regardless of size or composition.

Results

Quantitative, High-Throughput Measurements of Circulation Half-Life.

We have developed a quantitative microscopy-based high-throughput evaluation tool to standardize and accelerate the analysis of circulation half-life of fluorescently labeled IV-injected agents. In comparison to traditional plate-reader methods for measuring circulation half-life (*SI Appendix*, Fig. S1), the major strengths of this tool are: 1) precise blood concentration measurements can be made using only 2 μL of blood volume (0.1% of the total blood volume for a mouse); 2) multiple cohorts of experimental animals can be analyzed simultaneously; 3) this method allows for multiplexed analysis of diverse therapeutic agents and biological variables; and 4) continuous sampling from the same animal can reduce the number of animals necessary to make meaningful conclusions. A schematic of the workflow is illustrated in Fig. 1.

After systemic IV injection of a fluorescently labeled agent, such as dye-loaded polymeric NPs, 2 μL of blood was collected at the desired time points following injection. In total, typically ≤1% of the blood volume of an adult mouse was collected over the course of the experiment. During and after blood collection, other experimental end points may also be measured, such as imaging with an in vivo imaging system (IVIS) instrument for biodistribution. After blood collection, blood samples were dispensed into a 384-well glass-bottom plate along with a set of standards. Multiple images of each well in the plate could then be acquired using an automated epifluorescence imaging system. Fluorescence intensities of the collected images were then analyzed using
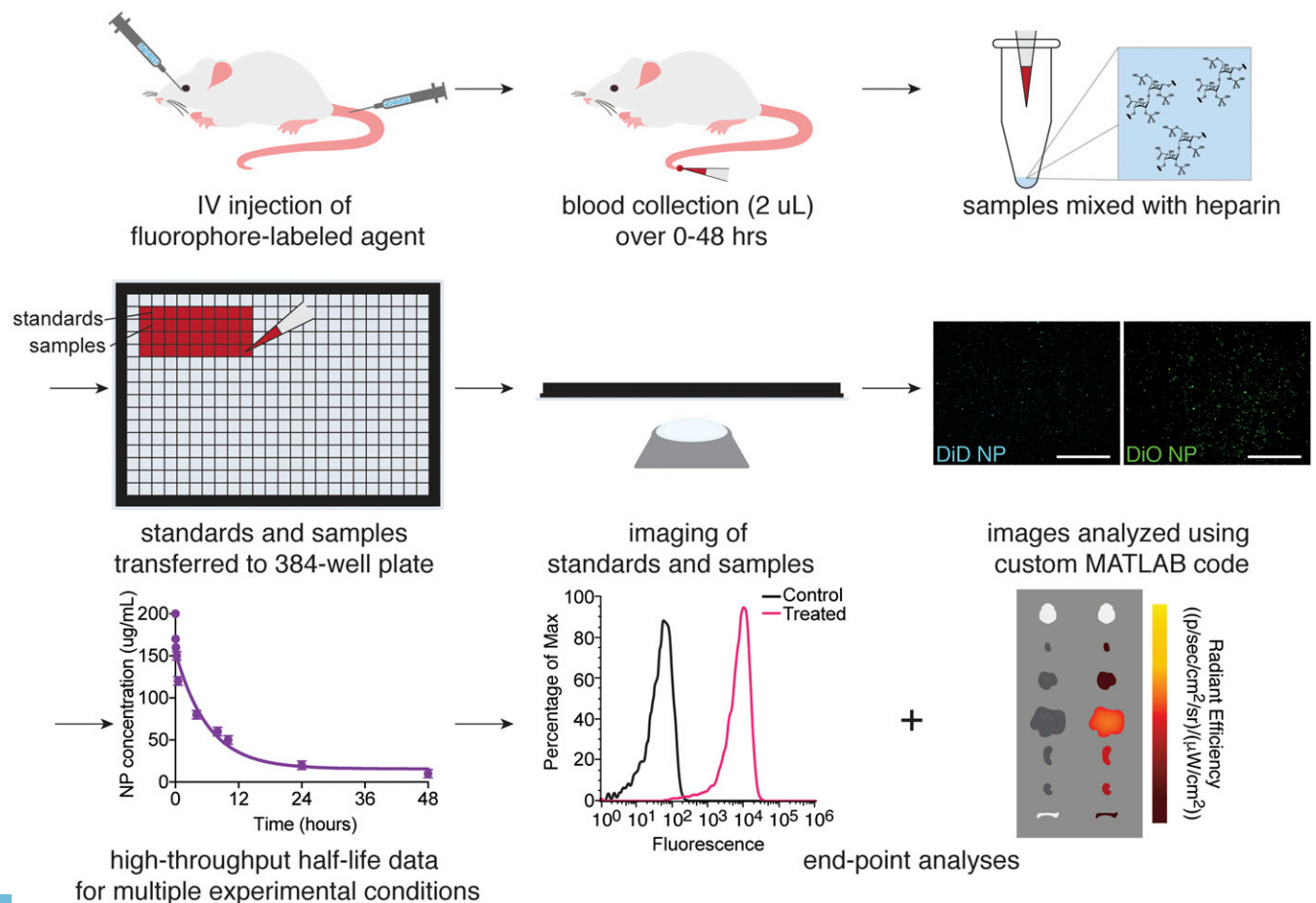
Fig. 1. Schematic illustrating the workflow for half-life measurements and end-point analyses using high-throughput quantitative microscopy.

Bracaglia et al.

www.manaraa.com

a custom MATLAB program, a workflow of which is illustrated in *SI Appendix,* Fig. S2, and compared to the standard curve to obtain the fluorescent agent concentration in blood for each sample.

Accurate Detection of Circulation Half-Life Following Different IV Routes of Administration. We first injected BALB/c mice with DiIC18 (5); 1,1′-dioctadecyl-3,3,3′,3′-tetramethylindodicarbocyanine, 4-chlorobenzenesulfonate salt (DiD)-loaded poly(lactic acid) (PLA)-polyethylene glycol (PEG) NPs (~170 nm in diameter, *SI Appendix,* Table S1) IV via either retro-orbital (RO) or tail-vein (TV) administration (Fig. 2*A*) to compare the circulating half-life measurements for the same agent via different routes of IV administration and as an initial proof-of-concept that consistent results could be obtained within an experimental cohort. Blood samples were collected from a tail nick. Fig. 2*B* shows fluorescence images of DiD-loaded PLA-PEG NPs in blood at two different concentrations, indicating a clear difference in the number of NPs and the resulting total fluorescence intensity. After blood collection and analysis using the high-throughput method, Fig. 2*C* shows the measured circulating NP concentrations for both routes of administration over time averaged across three mice. The NP circulation half-life was calculated as 5.2 h for RO and 5.6 h for TV. This result is consistent with an ~6-h circulation half-life reported in rats (17) and more recently with a 6.6-h circulation half-life reported in mice using C14-labeled PLA-PEG NPs (18). The average SD between animals in the same cohort across all time points was low [9.6 μg/mL (RO) and 15.4 μg/mL (TV)]. As an example of the variation between images and animals observed using the high-throughput method, *SI Appendix,* Table S2, contains NP concentration data calculated for each image of each blood sample per time point for this experiment. Interestingly, we observed some initial dissimilarities in NP concentration between the two administration routes within the first 30 min of collection (Fig. 2*C, Inset*). We measured an initially higher concentration in the TV samples that decreased over the first hour after administration,

whereas the RO samples increased in concentration over the first 30 min of collection, after which they exhibited similar values to the TV samples. This discrepancy is likely due to the fact that blood was sampled from the tail, and thus a higher initial NP concentration would be expected from the TV samples. NPs administered RO required some time to circulate before they could be detected from tail-nick blood sampling. These results suggest that even small differences in NP concentration can be accurately measured with the quantitative high-throughput method.

After blood collection, organs were harvested and imaged using an IVIS system and homogenized into a single-cell suspension for flow cytometry analysis of cellular NP uptake in the different tissues. Fig. 2 *D* and *E* demonstrate identical tissue uptake results after RO and TV administration with high levels of uptake in the liver and spleen, consistent with previous reports (19). Similarly, in Fig. 2*F*, IVIS imaging confirms that the highest fluorescence signal is found in both the liver and the spleen. Together, these results demonstrate the feasibility of accurately performing multiple experiments in the same research animals after IV NP injection while also completing the circulating half-life analysis since it uses only a small amount of blood volume per animal.

To confirm that tracking encapsulated dye accurately represents tracking the polymeric vehicle, we formulated NPs using Cy5-conjugated polymer loaded with DiIC18 (3); 1,1′-dioctadecyl-3,3,3′,3′-tetramethylindocarbocyanine (DiI) dye such that the polymer and the cargo could be imaged separately. We administered these dual-color NPs in vitro in human embryonic kidney 293 (HEK293) cells and IV in vivo and collected samples at various time points. Fluorescence imaging was used to determine whether the polymer and encapsulated dye colocalized (*SI Appendix,* Fig. S3). Furthermore, 48 h after NP administration in mice at our typical experimental end point, we sectioned their livers postmortem to determine whether fluorescence signals from the polymeric vehicle and the dye cargo colocalized in this organ. In both in vitro and in vivo samples, we observed
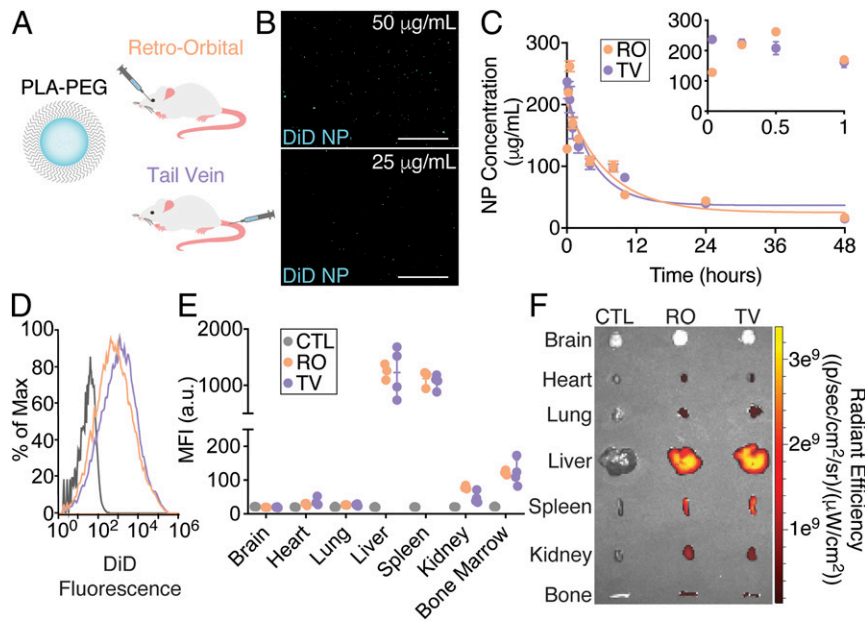

Fig. 2. Tail-vein and RO injections of polymeric nanoparticles yield identical measurements of half-life. (*A*) Schematic of polymeric nanoparticles composed of a PLA-PEG copolymer encapsulating fluorescent dye and routes of IV administration. (*B*) Representative fluorescence images of dye-loaded nanoparticles at different concentrations in blood. (*C*) Circulation half-life measurements after IV administration of fluorescent polymeric nanoparticles using quantitative microscopy (*n* = 3 mice per group per time point). Error bars represent SEM. Representative end-point (*D*) flow cytometry histograms from homogenized livers, (*E*) mean fluorescence intensity (MFI) values for homogenized organs (*n* = 3 to 4 mice per group per time point; error bars represent SEM), and (*F*) IVIS analyses of NP uptake in various tissues. (Scale bars, 100 μm.)

Bracaglia et al.

colocalization of polymer and dye signals, suggesting that using dye cargo as a tracer within the 48-h period used for our high-throughput protocol provides an accurate representation of the behavior of the polymeric vehicle.

Accurate Detection of Circulation Half-Life of Fluorescent Antibodies. In addition to fluorescently dyed NPs, this technique was also successfully implemented in the assessment of the concentration of a fluorescently labeled antibody in the circulating blood. In this experiment, mice received RO injections of fluorescently labeled mouse anti-human CD45 antibody (Fig. 3A and *SI Appendix*, Table S1). This antibody type (IgG) is commonly used experimentally for cell-labeling. From 2-μL blood draws over 48 h, the concentration of antibody remaining in the blood is shown in representative images in Fig. 3B and averaged across three mice in Fig. 3C. In Fig. 3B, a qualitative comparison shows higher levels of fluorescence in the blood at 15 min compared to blood collected at 10 h and that both experimental blood samples have distinct fluorescence compared to control blood. After correlating measured intensities using the concentration standard, the calculated concentrations were plotted versus time in Fig. 3C. The concentration profile shows an initial phase of constant concentration at approximately the injected dose (20 μg/mL). The concentration then slowly decreases after 1 h of circulation with a half-life of 34.4 h. This decay profile is expected from a species-matched antibody (20). At 48 h after the injection, organs from treated mice were analyzed using IVIS imaging (Fig. 3F), which shows minor fluorescence detections in the lung, liver, kidney, and bone. The organs were then homogenized and the fluorescence intensity of the cells within each organ was analyzed using flow cytometry (Fig. 3 D and E) and compared to cells from an untreated mouse. From this analysis, antibodies were found in cells from the liver and bone marrow, but not in the lung tissue. This result could indicate that antibodies have left the circulating blood and entered the interstitial space of the organ but have not associated directly with cells.

Simultaneous Analysis of Multivariable Experiments. To demonstrate the feasibility of completing multivariable experiments, we next used the quantitative high-throughput half-life method to measure the circulation half-life of dye-loaded PLA-PEG (~170 nm) or poly(lactic-co-glycolic acid) (PLGA) (~270 nm) NPs (Fig. 4A and *SI Appendix*, Table S1) after IV administration in both male and female mice in four cohorts totaling 12 mice. Following the procedures described above, 108 blood samples across nine time points from 12 mice were loaded into the same glass-bottom plate and imaged alongside PLA-PEG and PLGA NP concentration standards. Simultaneous imaging under the same conditions enables reliable and unbiased comparisons between experimental conditions. We observed a short half-life of 45 and 51 min for PLGA NPs in male and female mice, respectively (Fig. 4B). The blood circulation profile for PLGA NPs is consistent with previous results using In-111–labeled PLGA NPs in mice (21). We calculated a half-life of 6.3 and 6.6 h for the smaller PLA-PEG NPs in both male and female mice, respectively (Fig. 4C). The longer circulation time observed with PLA-PEG compared to PLGA is supported by the concept that circulation half-life increases with decreasing NP size and the incorporation of PEG on the NP surface (1). In addition to a multicohort experiment, our high-throughput protocol can also be used to compare multiple fluorescent agents within the same animal in a multiplexed fashion. To demonstrate this capability, we used the high-throughput method to measure the circulation half-life of DiI-loaded PLA-PEG NPs and DiD-loaded PLGA NPs coadministered into the same animals. As a confirmation that we were able to distinguish coadministered NP formulations loaded with DiI from those loaded with DiD, we observed distinct signals in HEK293 cells treated in vitro by flow cytometry, microscopy, and IVIS imaging (*SI Appendix*, Fig. S4 A–J). Following each formulation separately after coadministration in vivo allowed us to demonstrate the effects of multiplexing on the half-life of each individual formulation compared to isolated administration. While the general blood concentration profiles were similar for multiplexed and single administration, we calculated
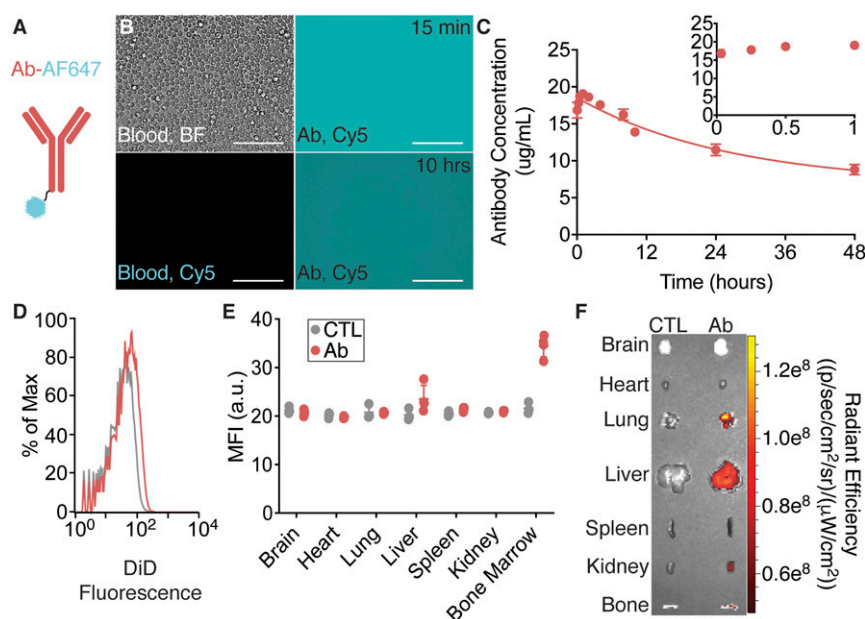
Fig. 3. Mouse antibodies remain in circulation for an extended time. (A) Schematic of a fluorescently labeled mouse anti-human CD45 antibody. (B) Representative phase-contrast and fluorescence images of blood with or without fluorescently labeled antibodies at different concentrations in blood. (C) Circulation half-life measurements after IV administration of fluorescently labeled antibodies using quantitative microscopy (n = 3 mice per group per time point). Error bars represent SEM. Representative end-point (D) flow cytometry histograms from homogenized livers, (E) MFI values for homogenized organs (n = 3 to 4 mice per group per time point; error bars represent SEM), and (F) IVIS analyses of NP uptake in various tissues. (Scale bars, 100 μm.)
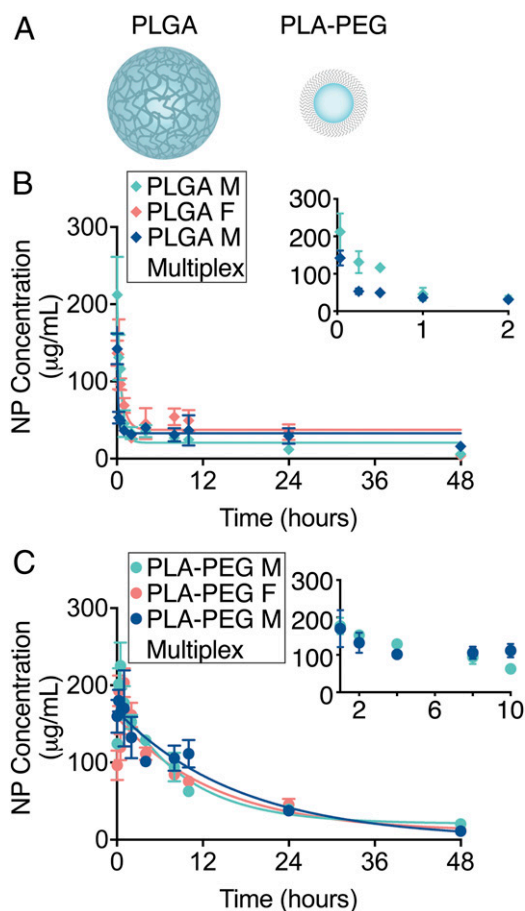
Bracaglia et al.

www.manaraa.com

Fig. 4. Nanoparticle size, surface chemistry, and multiplexed administration dictate circulation half-life and biodistribution. (*A*) Schematic of PLGA and PLA-PEG polymeric nanoparticles encapsulating fluorescent dye. Circulation half-life measurements following IV administration of (*B*) DiD-loaded PLGA nanoparticles and (*C*) DiD-loaded PLA-PEG nanoparticles in male (light blue) and female (light red) mice (*n* = 3 mice per group per time point), and in a multiplexed experiment (dark blue) where mice were simultaneously administered DiI-loaded PLA-PEG and DiD-loaded PLGA NPs using quantitative microscopy (*n* = 3 mice per group per time point). Error bars represent SEM.

differences in half-life for both PLGA and PLA-PEG NPs (Fig. 4 *B* and *C*). The insets in Fig. 4 *B* and *C* highlight these variations. The half-life for PLGA NPs was calculated as 21 min (roughly half of the value calculated following single administration). On the other hand, the half-life for PLA-PEG NPs increased to 8.5 h. These changes in the calculated half-life in a multiplex context are consistent with other studies that strategically administer multiple formulations to manipulate blood bioavailability of a particular formulation (22, 23). Interestingly, we also observed differences in biodistribution of PLA-PEG NPs (for example, decreased signal in the spleen) by IVIS imaging (*SI Appendix*, Fig. S4 *K–M*) coincident with variation in the blood clearance rate. Together, these results highlight the versatility of the quantitative high-throughput circulation half-life method and its applicability to experiments that simultaneously evaluate multiple fluorescent agents with minimal sample postprocessing while significantly reducing analysis time and investigator-related bias.

High-Throughput Method Has Reduced Sample Variation Compared to Other Methods. We compared NP concentration in the blood of four mice using the traditional method, the slide method we previously reported, and the high-throughput method described

here at a single time point (4 h) (Fig. 5*A*). The concentrations determined using each of the methods were similar, resulting in values between 222 and 176 μg/mL. However, the deviations between the six data points using each of these methods is highly varied with the traditional method resulting in a SD of ±56 μg/mL and the high-throughput method resulting in a SD of ±19 μg/mL (reducing the deviation by over 60%). The deviation between data points using the newly described method is similar to that found using the referenced slide method, which, to our knowledge, was the most accurate tool to assess NP blood concentration. This comparison shows that a similar accuracy can be obtained using the high-throughput method without the inclusion of a reference NP to account for thickness variation. The consistency between different areas of the sample using the high-throughput method is shown in call-out images (Fig. 5*D*) and compared to the variation between areas in the slide method (Fig. 5 *B* and *C*).

Discussion

Here we describe a versatile technique to measure the rate of disappearance of fluorescently labeled agents in blood circulation after systemic injection in vivo using quantitative fluorescence microscopy. This method is technically straightforward and requires only common laboratory equipment (a microscope, widely available software, and a commercially available glass plate). This approach makes two key technical improvements to traditional methods: improved accuracy with low sample volume and high-throughput processing. Highly accurate concentrations can be measured using only 2 μL of sampled blood per time point per animal, as evidenced by the reduced SD between measurements compared to previously published methods (Fig. 5). The low sample volumes required allow researchers to safely follow concentrations in the same animal from time point to time point over 48 h and also support additional end-point measurements as less than 1% of the blood is collected over this period. To support high-throughput processing, samples were frozen upon collection to be imaged using automated acquisition at a later time, reducing sample preprocessing steps. This also increases the allowable sample size in a single experiment both in terms of collection and analysis constraints. Additionally, the method reduces user error and the need for manual data acquisition and analysis. Minor limitations of the method include the following: fluorescently labeled agents need to be stable and uniformly distributed in the blood for accurate concentration determination; depending on the route of administration and the blood collection site, there may be a lag in achieving a homogeneous distribution in the blood, leading to potentially skewed results at
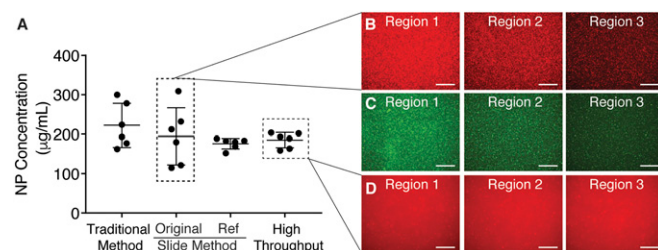

Fig. 5. A comparison of nanoparticle concentration using previous methods shows similar concentration with reduced deviation. (*A*) Circulation half-life measurement at a single time point (4 h) after IV administration of PLA-PEG nanoparticles using the traditional method to dissolve nanoparticles, the initial improved protocol moving to quantitative microscopy, and the high-throughput method described here (*n* = 6 images per group). Error bars represent SD. Images obtained through these techniques demonstrate the variation between regions imaged using a microscope slide (*B* and *C*) and the consistency obtained using a glass-bottom plate (*D*). (Scale bars, 100 μm.)

www.manaraa.com

initial time points; finally, the small collection volume is vulnerable to collection errors, although carefully adhering to the described protocol significantly reduces these errors. Overall, the described approach is a powerful tool that is easy to implement in a variety of contexts.

To validate this method, we have demonstrated the reliable assessment of concentration in the blood of a variety of fluorescent agents, including polymeric NPs and antibodies, over 48 h. Furthermore, we have shown the utility of the approach by including data from a multivariable, multicohort experiment. This technique is versatile both in terms of the variety of agents that can be assessed and the biological experimental parameters that can be implemented simultaneously. For example, less than 1% of blood and injected materials are removed over the course of the experiment. In the examples shown here, we demonstrate that thorough biodistribution analyses can be completed within the same experiment as circulating half-life analyses, highlighting the amount of information that can be gained from a single animal. If fluorescently labeled therapeutic agents are administered, we speculate that phenotypic assessments can also be made in experimental animals. Furthermore, we have demonstrated the use of this technique in mice, but it should be readily adaptable to other species as well. Similarly, this technique can be applied using any fluorescently labeled agent (for example, other NP types, peptides, antibody-drug conjugates, or small molecules). To apply this method to a broader range of unlabeled agents, a small fraction of fluorescently labeled agent could be spiked into an otherwise unlabeled therapeutic dose, given that this method enables accurate detection of even small concentrations in the blood (~1 μg/mL) of fluorescent agents.

As NP and other molecular-engineering technologies advance to support the generation of many varieties of delivery vehicles, there has been a growing interest in multiplexing experiments, or administering many delivery-vehicle varieties to the same animal to observe and directly compare vehicle behavior in vivo (24). Provided that a different fluorophore is used to label each class of delivery vehicle, the high-throughput method can also be used for multiplexed analysis, with the additional capability of assessing agents other than NPs. In Fig. 4, dye-loaded PLA-PEG or PLGA NPs were administered either separately into different mice or into the same mouse in a multiplexed version of this experiment. Coadministration yielded different half-life measurements compared to single administration. While multiplexing can provide a general sense of blood concentration profile, in this case coadministration of multiple agents did impact the kinetic behavior of each individual agent. The circulating concentration over time quantified by our high-throughput approach could add valuable temporal data on a single animal with relatively low additional effort to multiplexing experiments that otherwise only consider end-point measurements.

We anticipate that this method will facilitate preclinical screening of therapeutic agents and elucidate the relationship between their size/chemical structure and their physiological fate after IV administration. Blood circulation half-life is a powerful indicator of frequency of interaction with intended target tissues and cell types prior to elimination from the body (1, 2). On the whole, we believe that this method is of interest to a wide audience, particularly researchers studying the systemic delivery of therapeutics, diagnostic markers, and engineered NPs.

Materials and Methods

Materials. PLA-PEG polymer [16:5 PLA:PEG kilodaltons (kDa) molecular weight (MW)] was purchased from PolySciTech and used as received. PLGA polymer (50:50 DL-PLG, inherent viscosity 0.55 to 0.75 dL/g) was purchased from Lactel and used as received. PLGA-Cy5 polymer (50:50, 30 to 55 kDa MW) was purchased from PolySciTech and used as received. Ultra Pure dimethylsulfoxide (DMSO) was purchased from AmericanBio. Dichloromethane (DCM) (HPLC grade, +99%) was purchased from Sigma Aldrich. DiOC18 (3) 3,3'-dioctadecyloxacarbocyanine

perchlorate (DiO), DiD, and DiI dyes were purchased from Biotium and dissolved in DMSO at 10 mg/mL prior to use. Mouse anti-human CD45 Alexa Fluor 647 and mouse anti-human CD45 fluorescein isothiocyanate (FITC) antibodies were purchased from ThermoFisher Scientific. Heparinized Eppendorf tubes were purchased from ThermoFisher Scientific. Heparin [1,000 United States Pharmacopeia (USP)/mL] was purchased from Cardinal Health. Isoflurane was purchased from Sigma Aldrich. Glass-bottom 384-well plates were purchased from MatTek. Fisherbrand Superfrost Microscope slides were purchased from ThermoFisher Scientific.

NP Formulation and Characterization. PLA-PEG NPs were prepared by a nanoprecipitation procedure (16). Briefly, PLA-PEG polymer was dissolved in DMSO at a concentration of 50 mg/mL with 0.5% (wt/wt) of DiD, DiO, or DiI dye. The polymer and dye solution was added dropwise to diH$_2$O under vigorous agitation. NP size and zeta potential were measured via dynamic light scattering (DLS) (Malvern Instruments). NPs were then washed two to three times in diH$_2$O using filtered centrifuge tubes (Amicon Ultra 15 mL) to remove the organic solvent, after which NPs were aliquoted and flash-frozen in liquid N$_2$. One aliquot was lyophilized and weighed to determine the NP concentration. PLGA or PLGA-Cy5 NPs encapsulating DiD, DiO, or DiI were formulated using a single oil-in-water emulsion solvent evaporation technique as previously described (25). Briefly, 50 mg of polymer was dissolved in 900 μL of DCM overnight. One hundred microliters of DiD or DiO dye at 2.5 mg/mL in DMSO was added to the dissolved polymer immediately prior to formulation [0.5% (wt/wt)]. The polymer and dye solution was added dropwise under a vortex into 2 mL of 5% (wt/vol) low MW polyvinyl alcohol (PVA) solution and sonicated with a probe tip sonicator to form an oil-in-water single emulsion and then diluted into 10 mL of 0.3% (wt/vol) PVA solution while mixing. The remaining organic solvent was evaporated using a rotary evaporator. The NPs were then washed twice in diH$_2$O by centrifugation at 16,000 × g to remove excess PVA. NP size and zeta potential were measured via DLS. NP morphology was visualized by scanning electron microscopy (SEM). NP formulations were resuspended with 30 mg trehalose, lyophilized for at least 48 h, and stored at −20 °C.

Cell Culture and In Vitro NP Administration. HEK293 cells (ATCC) were cultured in 1:1 Dulbecco's Modified Eagle Medium/F12 medium supplemented with 10% fetal bovine serum (Atlanta Biologicals) and 50 μg/mL gentamicin. Cells were maintained in a 37 °C incubator in a humid 5% CO$_2$ atmosphere. To determine the extent of nanoparticle uptake in cultured cells, cells were seeded in 24-well glass-bottom tissue culture plates at a density of 50,000 cells/well in 500 μL of culture medium 24 h before NP treatment. Cells in each well were then treated with NPs at a concentration of 0.2 mg/mL. Uptake of NPs was quantified using flow cytometry (BD LSR II). Briefly, cells were washed three times with Dulbecco's phosphate-buffered saline (DPBS) 24 h after treatment, harvested, and resuspended in 2% bovine serum albumin (BSA) in PBS prior to analysis. All results were analyzed using FlowJo software. Uptake was further confirmed using fluorescence microscopy using an EVOS FL Auto 2 Cell Imaging System with standard red fluorescent protein (RFP) and Cy5 filters with an Olympus superapochromat 20×/0.75 numerical aperture (NA) objective, and an IVIS (Perkin-Elmer).

In Vivo NP Administration and Blood Collection. All animal procedures were performed in accordance with the guidelines and policies of the Yale Animal Resource Center and approved by the Institutional Animal Care and Use Committee of Yale University. Male and female BALB/c mice aged 4 to 6 wk old were used. Mice were anesthetized via vaporizer induction using isoflurane. Once respirations reduced to one breath/second, fluorescent agents were administered IV via an RO or tail-vein injection. Within 1 to 2 min after injection, a small tail nick was made with a sterile blade. Once animals were awake, blood samples (2 μL for high-throughput quantitative microscopy) were collected at 2, 15, and 30 min and at 1, 2, 4, 8, 10, 24, and 48 h following fluorescent agent injection with a p10 pipette from the tail nick. Sterile gauze was applied with pressure to the wound after blood collection to stop further blood flow. Blood volumes were promptly mixed 1:1 with both reference fluorescent agent and heparin (1,000 USP/mL) solution in heparinized tubes, and then the total mixed volume was diluted 1:1 with DPBS and flash-frozen on dry ice and stored at −80 °C until imaging and analysis. After 48 h, animals were killed by CO$_2$ inhalation. A cardiac puncture was used to draw blood postmortem.

Biodistribution End-Point Analyses. After IV injection of fluorescent agents, blood collection, and death as outlined above, animals were perfused transcardially with heparinized DPBS (100 USP/mL). Organs (brain, heart, lungs, liver, spleen, kidneys, bone) were harvested. Fluorescent agent

APPLIED BIOLOGICAL SCIENCES

ENGINEERING

accumulation in the organs was visualized and quantified using an IVIS (Perkin-Elmer). Tissues were then homogenized into a single-cell suspension through a 70-μm cell strainer and washed twice with PBS by centrifugation and resuspended in PBS containing 2% BSA. Uptake of fluorescent agents in single cells was analyzed by flow cytometry (Attune NxT) and compared to tissues harvested from untreated control animals. Liver biopsies from mice treated with PLGA-Cy5 DiI NPs were flash-frozen in optimal cutting temperature compound, sectioned, and imaged. Liver images were acquired using an EVOS FL Auto 2 Cell Imaging System with standard RFP and Cy5 filters with an Olympus superapochromat 20×/0.75 NA objective.

Traditional Half-Life Measurements with a Microplate. NPs were administered IV via RO injection. Larger blood volumes of 10 to 20 μL were collected by cardiac puncture at a single time point per animal for microplate analysis. A set of standards with a known NP concentration was also prepared in blood from control animals. After collection, blood samples were lyophilized. To dissolve the NPs, samples were resuspended in 1 mL acetonitrile and 100 μL DMSO and homogenized with a homogenizer. Homogenized samples were then centrifuged at $16,000 \times g$, and 800 μL of the supernatant was collected. The acetonitrile was evaporated using a SpeedVac, and the remaining DiD dye in DMSO was deposited into a microplate and analyzed using a plate reader (Ex/Em 644/670 nm). A schematic summarizing this method is shown in *SI Appendix*, Fig. S1.

Quantitative Microscopy Half-Life Measurements Using Slide Method. NPs were administered IV via RO injection, and blood was collected as described above after which NP concentration was assessed using quantitative microscopy as described previously (16). Briefly, blood samples were thawed and diluted 1:1 with DPBS, and 2 μL of each sample was spotted onto a microscope slide and covered with a 22-mm square coverslip. A set of standards with known DiD and reference DiO NP concentration was also prepared via serial dilutions in blood ranging from 0 to 250 μg/mL. All standards and samples were immediately imaged following slide preparation. At least six images per slide were collected. Images were acquired using an EVOS FL Auto 2 Cell Imaging System with standard green fluorescent protein and Cy5 filters with an Olympus superapochromat 20×/0.75 NA objective.

High-Throughput Half-Life Measurements and Data Analysis. Blood samples were thawed, and 10 μL of each sample was deposited into one well of a glass-bottom 384-well plate. A set of standards with known DiD or DiI and,

where applicable, reference DiO NP (or fluorescently tagged antibody) concentration was also prepared via serial dilutions in blood ranging from 0 to 250 μg/mL for NPs and 0 to 20 μg/mL for antibodies and deposited onto the plate. Images of all standard and sample wells were acquired using an EVOS FL Auto 2 Cell Imaging System with standard GFP, RFP, and Cy5 filters with an Olympus superapochromat 20×/0.75 NA objective. Six images per well in the middle of each well were acquired. Raw image files were saved for further analysis.

Data Analysis. To measure blood NP concentration using the microplate reader method, the fluorescence intensities from NP standards were used to plot a linear standard curve relating fluorescence intensity to NP concentration and determine the concentration of NPs in experimental samples. Results were analyzed using GraphPad Prism (version 8.1.2). For quantitative microscopy methods (slide method and high-throughput method), raw images were analyzed using a custom MATLAB code, a schematic of which is shown in *SI Appendix*, Fig. S2. Briefly, the intensity values of sample fluorophores (DiD or Alexa Fluor 647) and reference fluorophores (DiO or FITC) from each standard or sample image were summed, and the background for each channel (blood only) was subtracted. Then, either sample fluorophore intensity values or normalized sample fluorophore/reference fluorophore intensity values for the images corresponding to each standard or sample were averaged. Standards were used to plot a linear standard curve in GraphPad Prism relating fluorescence intensity to NP/antibody concentration and to determine the concentration of NPs/antibodies in experimental samples. For complete half-life experiments, concentration values for each blood sample per time point per animal were then plotted and fit to a one-phase decay curve in GraphPad Prism to determine circulating half-life values.

Data Availability. All data and protocols discussed in the paper are available in the main text or *SI Appendix*.

1. N. Hoshyar, S. Gray, H. Han, G. Bao, The effect of nanoparticle size on in vivo pharmacokinetics and cellular interaction. *Nanomedicine (Lond.)* **11**, 673–692 (2016).
2. Y. Deng *et al.*, The effect of hyperbranched polyglycerol coatings on drug delivery using degradable polymer nanoparticles. *Biomaterials* **35**, 6595–6602 (2014).
3. S. D. Gillies *et al.*, Improved circulating half-life and efficacy of an antibody-interleukin 2 immunocytokine based on reduced intracellular proteolysis. *Clin. Cancer Res.* **8**, 210–216 (2002).
4. Z. Elgundi, M. Reslan, E. Cruz, V. Sifniotis, V. Kayser, The state-of-play and future of antibody therapeutics. *Adv. Drug Deliv. Rev.* **122**, 2–19 (2017).
5. B. V. Ayyar, S. Arora, R. O'Kennedy, Coming-of-age of antibodies in cancer therapeutics. *Trends Pharmacol. Sci.* **37**, 1009–1028 (2016).
6. A. Beck, L. Goetsch, C. Dumontet, N. Corvaïa, Strategies and challenges for the next generation of antibody-drug conjugates. *Nat. Rev. Drug Discov.* **16**, 315–337 (2017).
7. K. G. Anderson *et al.*, Intravascular staining for discrimination of vascular and tissue leukocytes. *Nat. Protoc.* **9**, 209–222 (2014).
8. C. Glaus, R. Rossin, M. J. Welch, G. Bao, In vivo evaluation of (64)Cu-labeled magnetic nanoparticles as a dual-modality PET/MR imaging agent. *Bioconjug. Chem.* **21**, 715–722 (2010).
9. A. Ruiz *et al.*, Short-chain PEG molecules strongly bound to magnetic nanoparticle for MRI long circulating agents. *Acta Biomater.* **9**, 6421–6430 (2013).
10. NIH Office of Intramural Research, Animal Research Advisory Committee Guidelines: Guidelines for Survival Bleeding of Mice and Rats (NIH, 2015).
11. M. W. McGuill, A. N. Rowan, Biological effects of blood loss: Implications for sampling volumes and techniques. *ILAR J.* **31**, 5–20 (1989).
12. S. Krishnamurthy *et al.*, Surface protein engineering increases the circulation time of a cell membrane-based nanotherapeutic. *Nanomedicine (Lond.)* **18**, 169–178 (2019).
13. L. B. Mensah *et al.*, Layer-by-layer nanoparticles for novel delivery of cisplatin and PARP inhibitors for platinum-based drug resistance therapy in ovarian cancer. *Bioeng. Transl. Med.* **4**, e10131 (2019).
14. F. Yoshino *et al.*, Preferential tumor accumulation of polyglycerol functionalized nanodiamond conjugated with cyanine dye leading to near-infrared fluorescence in vivo tumor imaging. *Small* **15**, e1901930 (2019).
15. Z. Popović *et al.*, A nanoparticle size series for in vivo fluorescence imaging. *Angew. Chem. Int. Ed. Engl.* **49**, 8649–8652 (2010).
16. G. T. Tietjen, J. DiRito, J. S. Pober, W. M. Saltzman, Quantitative microscopy-based measurements of circulating nanoparticle concentration using microliter blood volumes. *Nanomedicine (Lond.)* **13**, 1863–1867 (2017).
17. T. Verrecchia *et al.*, Non-stealth (poly(lactic acid/albumin)) and stealth (poly(lactic acid-polyethylene glycol)) nanoparticles as injectable drug carriers. *J. Control. Release* **36**, 49–61 (1995).
18. J. Hrkach *et al.*, Preclinical development and clinical translation of a PSMA-targeted docetaxel nanoparticle with a differentiated pharmacological profile. *Sci. Transl. Med.* **4**, 128ra39 (2012).
19. J. Wu *et al.*, Polyethylene glycol-polylactic acid nanoparticles modified with cysteine-arginine-glutamic acid-lysine-alanine fibrin-homing peptide for glioblastoma therapy by enhanced retention effect. *Int. J. Nanomedicine* **9**, 5261–5271 (2014).
20. P. Polakis, Antibody drug conjugates for cancer therapy. *Pharmacol. Rev.* **68**, 3–19 (2016).
21. R. Gref *et al.*, Biodegradable long-circulating polymeric nanospheres. *Science* **263**, 1600–1603 (1994).
22. T. Liu, H. Choi, R. Zhou, I. W. Chen, RES blockade: A strategy for boosting efficiency of nanoparticle drug. *Nano Today* **10**, 11–21 (2015).
23. M. Germain *et al.*, Priming the body to receive the therapeutic agent to redefine treatment benefit/risk profile. *Sci. Rep.* **8**, 4797 (2018).
24. J. E. Dahlman *et al.*, Barcoded nanoparticles for high throughput in vivo discovery of targeted therapeutics. *Proc. Natl. Acad. Sci. U.S.A.* **114**, 2060–2065 (2017).
25. R. L. McCall, R. W. Sirianni, PLGA nanoparticles formed by single- or double-emulsion with vitamin E-TPGS. *J. Vis. Exp.*, 51015 (2013).

www.manaraa.com